JOURNAL OF MATERIALS SCIENCE 26 (1991) 5543–5546

Effect of microstructure on the erosion and impact damage of sintered silicon nitride

J. E. RITTER, S. R. CHOI, K. JAKUS
Mechanical Engineering Department, University of Massachusetts, Amherst, Massachusetts 01003, USA

P. J. WHALEN
Allied Signal Research and Technical Center, Morristown, New Jersey 07960, USA

R. G. RATEICK, Jr.
Allied-Signal Aerospace Co., Bendix Division, South Bend, Indiana 46620, USA

The erosion rates and impact damage of two sintered silicon nitride materials with identical compositions but different microstructures were determined as a function of impacting particle (SiC) kinetic energy and temperature (25–1000 °C) using a slinger-type erosion apparatus. The coarse-grained silicon nitride had significantly better resistance to impact damage than the fine-grained material. Crack–microstructure interactions were characterized using scanning electron microscopy and showed that crack-bridging was an important toughening mechanism in the coarse-grained material. Post-impact strength data were significantly less than those predicted from the indentation–strength data, due to impact flaws linking up prior to fracture. Consistent with its greater fracture resistance, the erosion rate of the coarse-grained material was less than that of the fine-grained material for erosion at 25 deg, and was independent of erosion temperature.

1. Introduction

Ceramics are susceptible to localized surface cracking when subjected to impact by hard, sharp particles. It is generally believed that sharp-particle impact damage in ceramics can be modelled by the idealized flaw system produced by a sharp indenter such as Vickers [1–3]. The sharp indenter produces two distinctive crack systems: radial cracks that are responsible for strength degradation, and lateral cracks that are the source of material removal. The indentation fracture mechanics model predicts the extent of cracking in terms of indentation load (or impact energy) and target material properties (toughness, hardness and elastic modulus). The indentation fracture mechanics model has recently been extended to include sharp-particle impact damage of ceramics that exhibit crack resistance toughening [4].

This study examines the influence of the microstructure of two sintered silicon nitrides on resistance to sharp-particle impact damage. The erosion rate and post-impact strength were measured as a function of impacting particle (SiC) kinetic energy and temperature (25–1000 °C) using a slinger-type apparatus.

2. Experimental procedure

The two sintered silicon nitride materials studied here have the same composition, about 6.4 vol % of an amorphous yttria-based grain-boundary phase. This composition can be pressureless sintered to 99% theoretical density to produce a fine-grained silicon nitride, designated AS44. The microstructure of AS44 is characterized by a bimodal distribution of acicular grains. The coarse grains are about 0.8 μm in diameter and 6 μm in length, and comprise about 15 vol % of the material. The finer grains are about 0.07 μm in diameter and 1.0 μm long, and form the matrix of the material. Any residual porosity is finely distributed. The second material, designated AS440, is prepared by annealing the AS44 material at a high temperature to coarsen the microstructure. The coarse grains in the AS440 material are about 5 μm in diameter and about 40 μm in length. The fine-grained matrix also coarsens during annealing to about 1 μm in diameter and 6 μm in length. The residual porosity in the AS440 material results from the coalescence of the finely divided pores in the AS44 material. These porous regions, as large as 1 μm in size, are distributed throughout the material and have the shape of "snowflake-like" dendrites. The dendrites are not interconnected and AS440 has the same overall density as AS44. The specimens for this study were prepared from slip-cast billets of AS44/440 material and were in the form of discs (40 mm diameter and 2 mm thick) for the impact samples and bars (3 by 6 by 50 mm) for the indentation tests. These samples were ground down to a surface finish of better than 0.4 μm on the impact/indent face. The fracture toughness of the samples was measured by the short rod, chevron notch technique [5]. For AS44, the fracture toughness was 5.75 MPa m^{-2} and for AS440

0022–2461/91 $03.00 + .12

8.30 MPa m^{-2}. The elastic modulus for AS44 was 310 GPa and its hardness is 15.6 GPa. For AS440 the elastic modulus is 365 GPa and hardness 14.0 GPa.

Indents for subsequent strength testing were placed on the centre of the tensile surface of the specimen, and the indent impression and radial crack size measurements were taken immediately after indentation. The samples were indented with a Vickers diamond indenter over a load range of 30–200 N. Three samples per indentation load were used.

Multiparticle impact tests (5 samples per test condition) at normal incidence were conducted in air at 25, 800 and 1000 °C using a slinger type apparatus as described in [6]. In this apparatus, commercial-grade SiC particles are fed into the centre of a 50.8 cm diameter tubular rotor rotating in a horizontal plane, are accelerated to the end of the tube, and leave the rotor to strike specimens that are positioned around the perimeter of the apparatus. In this study, two particle speeds of 37 m s^{-1} and 80 m s^{-1} were used in combination with two grit sizes (1015 and 360 μm diameter) to give four different impacting kinetic energies. The erosion rate, defined here as the volume loss per particle impact, was calculated from the mass loss by the sample and an estimate of the number of particles impacting the sample [4].

After indentation or impact the samples were strength tested at room temperature in air at a fast crosshead speed with the eroded/indent surface covered with mineral oil to minimize any fatigue effects. The indentation samples were tested in four-point bending with an inner span of 20 mm and an outer span of 40 mm. The impact samples were tested in a ring-on-ring biaxial bending fixture and the appropriate equation to calculate fracture strength is given in [7]. After strength testing, fractographic analysis was carried out to ensure that the strength-controlling flaw was that produced by indentation or impact.

3. Results and discussion

Both silicon nitrides exhibited the classical indentation pattern: indent impression with radial cracks emanating from the four corners of the indent. However, with AS440 the radial crack path was irregular and predominantly intergranular (see Fig. 1). The impact damage sites were similar to the indentations with both radial and lateral cracks surrounding the impact site (Fig. 2).

Fig. 3 summarizes the post-indentation strength data. By assuming that fracture resistance, K_R, depends on crack size, C, by [4]

$$K_R = kC^m \quad (1)$$

Post-indentation strength (σ_f) can be derived to be related to the indentation load (P) by [4]

$$\sigma_f = (k/Y)\left(\frac{3 + 2m}{4}\right) \times [4\chi P/k(1 - 2m)]^{(2m-1)/(2m+3)} \quad (2)$$

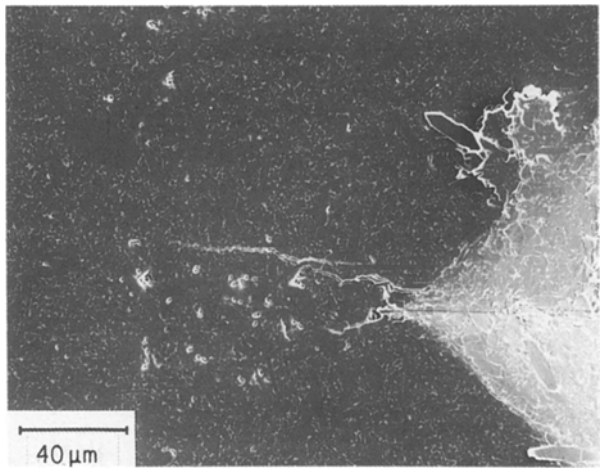

Figure 1 Vickers indentation in AS440. Indentation load $P = 185$ N.

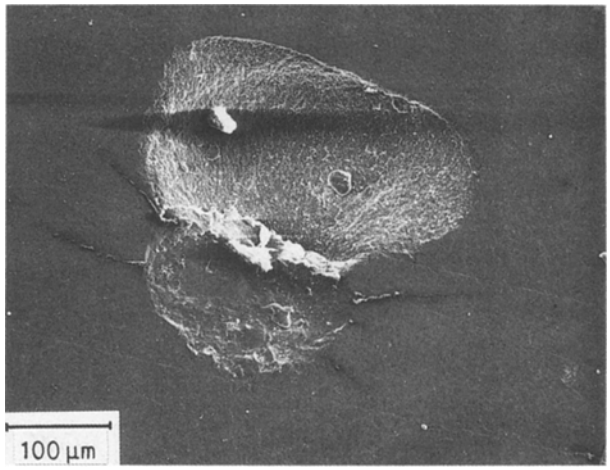

Figure 2 Isolated particle impact in AS44. Impacting kinetic energy $U_k = 1942$ μJ.

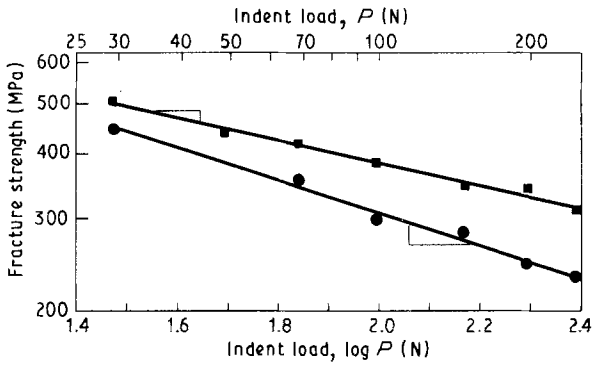

Figure 3 Average post-indentation strength as a function of indentation load. The solid line represents the best-fit line with slope β. ■, AS44: β = −0.3146; $m = 0.0214$. ●, AS440: β = 0.219; $m = 0.141$. $\sigma_f \propto P^\beta$; $\beta = (2m - 1)/(2m + 3)$.

where k and m are fracture resistance constants, χ is an indent residual stress constant, and Y is a flaw shape parameter, equal to 1.128 for a semicircular flaw. Based on Equation 2, m can be determined from the best-fit slopes of the curves (β) in Fig. 3. For AS440, m was calculated to be 0.141, and for AS44, 0.0214. The significantly higher m for AS440 is indicative of the greater crack resistance toughening of this material.

The fracture resistance curves for these two materials can be determined by substituting into Equation 1 the chevron-notch toughness and assuming that this toughness is reached at a crack size of 1000 μm. The predicted fracture resistance curves are summarized in Fig. 4. It is evident that the coarser microstructure of AS440 leads to a significantly greater fracture resistance. This influence of microstructure on fracture resistance is consistent with previous results where it was found that silicon nitride [8] and alumina [4] with large grain sizes exhibited strong crack-resistance toughening. It is believed that the coarser microstructure, especially with the bimodal grain size, leads to the irregular, tortuous crack path in AS440 and that this in turn enhances crack bridging by leaving unbroken grains behind the crack tip. The cumulative effect of the crack bridges setting up closure stresses behind the crack tip leads to crack resistance toughening [9].

The indentation results in Fig. 3 can be used to predict the post-impact strength results. Assuming that the impact event can be modelled as a quasi-static indentation, the relationship between impacting particle kinetic energy (U_k) and equivalent indentation load is [10]

$$P = \alpha \xi H^{1/3} U_k^{2/3} \quad (3)$$

where α is a constant related to the fraction of energy transferred to the target material, ξ is an indenter constant equal to 4.8 for the Vickers geometry, and H is hardness. Substituting Equation 3 into Equation 2 gives the post-impact strength as a function of kinetic energy:

$$\sigma_f = (k/Y)(3 + 2m)/4 \times \left[\frac{4\chi(\alpha \xi H^{1/3} U_k^{2/3})}{k(1 - 2m)}\right]^{(2m-1)/(2m+3)} \quad (4)$$

Based on Equation 4, the slope of the $\sigma_f - U_k$ curve on logarithmic axes should be equal to two-thirds $(2m - 1)/(2m + 3)$.

Figs 5 and 6 compare the post-indentation strength data to the post-impact strength data for AS44 and AS440, respectively. Note that Equation 3 was used to relate the U_k and P scales in Figs 5 and 6, assuming $\alpha = 1.0$ and $\xi = 4.8$. It is evident that the m values determined from the post-impact strength data are significantly greater than those determined from the post-indentation strength data. However, it is important to note that, consistent with the post-indentation strength data, AS440 exhibits a greater resistance to impact damage than AS44.

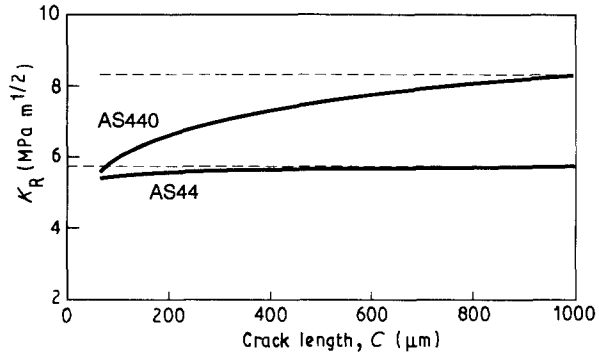

Figure 4 Predicted fracture resistance curves. AS44: $CNK_{IC} = 5.75$ MPa m$^{1/2}$. AS440: $CNK_{IC} = 8.3$ MPa m$^{1/2}$. $K_R = k(c)^m$.

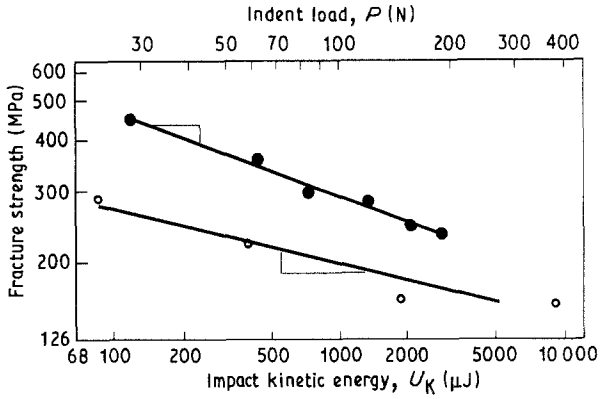

Figure 5 Comparison of post-impact and post-indentation strength data for AS44. The solid line represents the best-fit line with slope β. Indentation load was related to impact kinetic energy by $P = 4.8 H^{1/3} U_k^{2/3}$. ●, Indent data: $\beta = -0.315, m = 0.021$; ○, impact data; $\beta = -0.211, m = 0.151$.

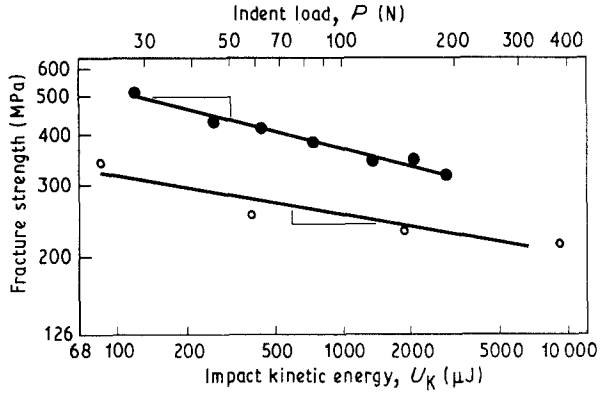

Figure 6 Comparison of post-impact and post-indentation strength data for AS440. The solid line represents the best-fit line with slope β. Indentation load was related to impact kinetic energy by $P = 4.8 H^{1/3} U_k^{2/3}$. ●, Indent data: $\beta = 0.219, m = 0.141$; ○, impact data: $\beta = 0.142, m = 0.251$.

The geometric irregularity of the impacting "sharp" particle can cause it to hit on an edge or face rather than a "sharp" point. This would cause less energy to be transferred and would also be expected to affect both the indenter constants χ and ξ as well as the crack geometry parameter Y. All of these factors taken together would lead to the conclusion that the post-indentation strength data in Figs 5 and 6 should represent a lower bound for the post-impact strength data. However, Figs 5 and 6 show that the post-impact strength data is significantly lower than the post-indentation strength data. We believe that the inability of the post-indentation data to accurately reflect the post-impact strength data is related to multiple impact flaws linking up prior to final fracture (see Fig. 7). Examination of the fracture origins in all the post-impact strength samples showed that two or more impact flaws were adjacent to one another at the fracture origin. Thus it is likely that these flaws linked up prior to final fracture and caused the lower than expected strengths of the post-impact data [11].

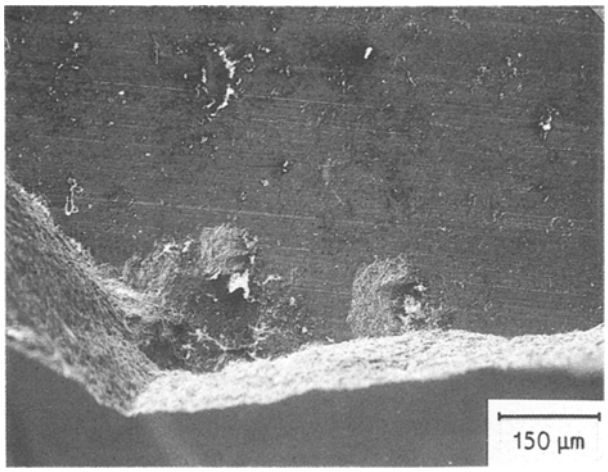

Figure 7 Fracture origin in AS440 showing multiple impact flaws linking up prior to final fracture.

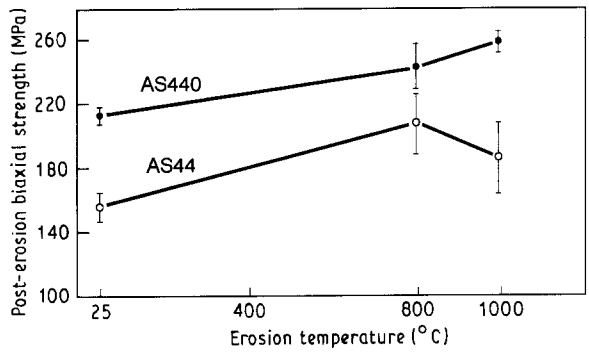

Figure 8 Post-impact strength as a function of temperature for an impacting kinetic energy of 9080 μJ. C.L. ± 95%. U_k = 9080 μJ.

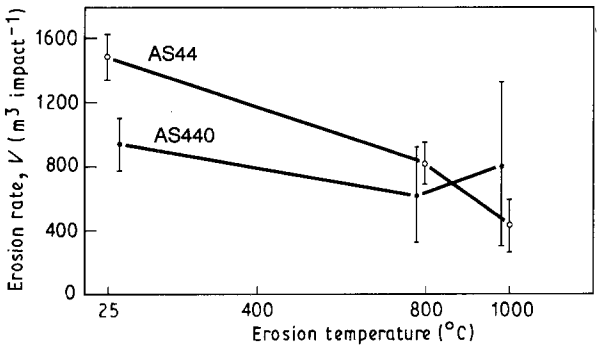

Figure 9 Erosion rate as a function of erosion temperature for an impacting kinetic energy of 5712 μJ. C.L. ± 95%. U_k 5712 μJ.

Fig. 8 shows the post-impact strength as a function of erosion temperature. From these results it can be seen that the post-impact strengths are somewhat higher after high temperature erosion than after erosion at 25 °C. These results indicate that the major influence of the erosion temperature is to help relieve the residual stress around the impact zone.

The erosion rate data as a function of erosion temperature are summarized in Fig. 9. Consistent with its greater fracture resistance, the erosion rate of AS440 at 25 °C is less than that of AS44. Although erosion temperature has little effect on the erosion rate of AS440, the erosion rate of AS44 continuously decreases with increasing erosion temperature, so that at 800 and 1000 °C the erosion rate of AS44 is about the same as that of AS440. Unfortunately, erosion rate data are not as amendable to indentation fracture mechanics analysis as are strength data, because lateral cracking is not the sole means for material removal. It was also observed in these materials that material removal occurred by extensive grain boundary cracking and subsequent grain fall-out. Thus, it is possible that the decrease in erosion rate for the AS44 material at high erosion temperatures is due to a change in the primary material removal mechanism.

4. Conclusions

A large acicular grain microstructure in sintered silicon nitride gives rise to fracture resistance toughening that leads to an increased resistance to post-impact strength degradation. Post-impact strength is significantly lower than post-indentation strength, due to the possibility of impact flaws linking up prior to final fracture. Consistent with its greater fracture resistance, the erosion rate of coarse-grained sintered silicon nitride is lower than the fine-grained material at 25 °C erosion, and is independent of erosion temperature. The erosion rate of the fine-grained material decreases with temperature.

References

1. D. B. MARSHALL, in "Nitrogen Ceramics", edited by F. L. Riley (Martinus Nijhoff, The Hague, 1983) p. 635.
2. B. R. LAWN, B. J. HOCKEY and H. RICHTER, *J. Microsc.* **130** (1983) 295.
3. J. E. RITTER, P. STRZEPA and K. JAKUS, *Phys. Chem. Glasses* **25** (1984) 159.
4. K. BREDER, J. E. RITTER and K. JAKUS, *J. Amer. Ceram. Soc.* **71** (1988) 1154.
5. J. H. UNDERWOOD, S. W. FREIMAN and F. I. BARRATTA (eds), "Chevron-Notched Specimens, Testing, and Stress Analysis", ASTM-STP 855 (ASTM, Philadelphia, 1984).
6. J. E. RITTER, P. STRZEPA, K. JAKUS, L. ROSENFELD and K. J. BUCKMAN, *J. Amer. Ceram. Soc.* **67** (1984) 769.
7. D. H. SHETTY, A. R. ROSENFELD, P. McGUIRE, G. K. BANSAL and W. H. DUCKWORTH, *Amer. Ceram. Soc. Bull.* **59** (1980) 1193.
8. C. W. LI and J. YAMANIS, *Ceramic Engineering Science Proceedings* **10** (1989) 632.
9. Y. W. MAI and B. R. LAWN, *J. Amer. Ceram. Soc.* **70** (1987) 289.
10. S. M. WIEDERHORN and B. R. LAWN, *ibid.* **62** (1979) 66.
11. J. E. RITTER and R. DAVIDGE, *ibid.* **67** (1984) 432.

Received 10 May
and accepted 26 June 1990